Remote Sensing Applications: Society and Environment 16 (2019) 100269

Contents lists available at ScienceDirect

Remote Sensing Applications: Society and Environment

journal homepage: http://www.elsevier.com/locate/rsase

Assessment of sedimentation process in flood water spreading system using IRS (P5) and supervised classification algorithms (case study: Dahandar plain, Minab city, south of Iran)

Maryam Abbaszadeh, Rasool Mahdavi *, Marzieh Rezai

Natural Resources Engineering Group, Faculty of Agriculture and Natural Resources Engineering, University of Hormozgan, Bandar Abbas, Iran

ARTICLE INFO

Keywords:
Overall accuracy
Regression
Maximum likelihood
Minimum distance
Parallelepiped

ABSTRACT

Many parts of Iran are dry plains that seem suitable places for building flood spreading systems and diverting flash floods to infiltration areas in order to recharge ground water resources. After passing a period of time, sediment deposition decreases the artificial recharge capacity of flood spreading system infiltration basins. Panchromatic images of IRS(P5) satellite are appropriate tools for studying sediment distribution, texture and thickness on the surface of these systems. For monitoring sediment distribution, the panchromatic images used that were taken in 2007,2010 and 2016. For evaluating sediment texture and thickness, 40 samples were collected from surface soil of different places all over Dahandar flood spreading system, in Minab city. By using Hydrometer method and soil texture triangle, different percentages of sand, silt, clay, soil texture types and sediment thickness were determined. Then by using simple linear regression the relationship between different percentages of sand, silt, clay and sediment thickness with the digital numbers of 2016 Panchromatic image were evaluated. The values of R^2 for sand, silt, clay and sediment thickness were 0.428, 0.343, 0.227 and 0.429 respectively. Different algorithms of supervised classification (maximum likelihood, minimum distance, parallelepiped) were used for creating maps with different classes of sand, silt, clay, soil texture types and sediment thickness. For sand particles, maximum likelihood algorithm with over all accuracy of 64%, for silt particles minimum distance-raw algorithm with over all accuracy of 51%, for clay particles minimum distance-normalized with over all accuracy of 46% showed the greatest values. For sediment thickness, different algorithms had the same function. The mentioned methods could reasonably explain the distribution of sand, silt and clay particles, soil texture and sediment thickness all over the flood spreading system.

1. Introduction

During recent decades, demand for water has increased and Unfortunately the level of underground water resources has declined because of overusing of them, so improving these water resources is totally necessary. A flash flood can be optimally harvested and stored in the ground through artificial recharge and flood water harvesting techniques (Hashemi et al., 2013). Flood spreading systems lead the water into underground water tables and recharge them, so they optimize usage of flood water (Hashemi et al., 2013; Moghanlou and Oskouei, 2007). These systems have different hydraulic components. A conveyance channel transfer water from an ephemeral river to flood spreading systems. The water of the ephemeral river is diverted to this channel by means of a diversion dam that is built on the ephemeral river. After passing through conveyance channel, water inters into spreading channel and several serial inter connected basins (Fig. 2). When flood flow inters the basins, it slows down or stops and the sediment load deposits. As the water goes through downstream basins, it becomes more clear, because most of the sediment load deposits in the first basins (Hashemi et al., 2013; Kowsar, 1991; Zarkesh, 2005). Unfortunately, sediment deposition decreases the artificial recharge capacity of infiltration basins. During flash floods, sediment deposition process is totally different from those in permanent rivers (Malmon et al., 2004). The basin infiltration rate depends on the sediment texture. Coarse-grained sediments have better recharge rates than fine-grained layers (Fennemore et al., 2005).Alexandridis et al., 2015; Ali et al., 2018; Allam et al., 2019; Bahadur Kc, 2009; Bartholdy and Folving, 1986; Bouyoucos, 1936; Congalton, 1991; Demattê et al., 2016; Duda and Canty, 2002;

* Corresponding author.
E-mail address: ra_mahdavi2000@hormozgan.ac.ir (R. Mahdavi).

https://doi.org/10.1016/j.rsase.2019.100269
Received 15 May 2019; Received in revised form 29 September 2019; Accepted 2 October 2019
Available online 4 October 2019
2352-9385/© 2019 Elsevier B.V. All rights reserved.

Fennemore et al., 2005; Gaber et al., 2009, 2015; Hashemi et al., 2013; He et al., 2009; Hoppus et al., 2002; Jimenez et al., 2005; Kowsar, 1991; Kumar et al., 2016; Lagacherie et al., 2008; Li et al., 2014; Liao et al., 2013; Licciardi et al., 24AD; Lilhare et al., 2014; Lu et al., 2004; Lu and Weng, 2007; Malmon et al., 2004; Mei et al., 2005; Moazami and Zoratipour, 2016; Moghanlou and Oskouei, 2007; Moslemi et al., 2017; Mostafaei et al., 2016; Muller and van Niekerk, 2016; Munyati, 2019; Nanni and Demattê, 2006; Rao et al., 2002; Richards, 1999; Shaharum et al., 2018; Small et al., 2009; Tempfli et al., 2009; Vasava et al., 2019; Zarkesh, 2005 After each flash flood, dispersion and thickness of basin sediments increase. So desiltation operation for improving the efficiency of the basin infiltration and prevention of damages to these systems is necessary. It can be concluded that, assessment of sediment dispersion, texture and thickness on these systems is so important.

Optical/thermal imagery provides continuous and updated information about temporal and spatial changes in areas that are subject to sediment deposition at different scales. Variations in reflected radiance from areas of deposited sediments can be resulted from changes in sediment texture and lithology (Nanni and Demattê, 2006; Small et al., 2009). Classification algorithms are often evaluated to find the best change detection results for a specific application (Lu et al., 2004; Lu and Weng, 2007; Munyati, 2019; Shaharum et al., 2018). Unsupervised classification plays an especially important role when very little a priori information about the studying area is available. This method attempts to organize the data into classes sharing similar, i.e. spectrally homogeneous, characteristics and uses them as information to discriminate between different unsupervised classes. It should be considered that there might be some errors in pixel spectral homogeneity (Duda and Canty, 2002). But in supervised classification by using information extraction from sources such as field or existing maps, representative pixels for each of the desired classes in the image are selected as training sites. Training areas correspond to each classification item ((Bahadur Kc, 2009; Jimenez et al., 2005). This kind of classification seems to be more suitable for discriminating more detailed characteristics of surface area. Although a lot of image classification algorithms have been proposed till now, commonly used supervised classification approaches are parallelepiped, minimum distance and maximum likelihood. They are easy to understand and implement. Classification algorithms have utilized for studying surface sediment in different environments (Bartholdy and Folving, 1986; Demattê et al., 2016; Gaber et al., 2009, 2015).

Moazami and Zoratipour (2016) Divided Jarmeh flood spreading system into 3 classes: areas with sediment deposition, intact soils and soils with changes. Then by using maximum likelihood algorithm they Monitored sedimentation process on flood spreading system during 13 years. The overall accuracy was 85% for the best image representing sedimentation process. Gaber et al. (2015) used classification algorithms and Six different satellite datasets to characterize the surface sediments in desert areas. The best overall accuracy and dataset was the supervised classification using the complex coherent matrix of the full polarimetric Radarsat-2 which was 96.43%. Madden et al. (2013) generated environmental faces map of an isolated fringing reef system by using unsupervised classification processes, Landsat image, field and petrographic studies. An overall accuracy of pixel classification linked to environmental faces of 71% was indicative of good agreement across the Landsat generated faces map.

Besides classification techniques, other statistical methods like regression analysis can estimate field properties by using reflectance values (He et al., 2009; Mostafaei et al., 2016; Muller and van Niekerk, 2016; Vasava et al., 2019). Regression analysis can be used for estimating soil texture by using soil reflectance measurements. Liao et al. (2013) evaluated Spatial estimation of surface soil texture using remote sensing data in agricultural regions. In the study, they used multiple stepwise regression (MSR) based on the relationship between surface soil sand, silt and clay contents and the DNs of Band 7 ETM remote sensing data. The R^2 values of the regression analysis were 0.32, 0.21 and 0.36 for sand, silt and clay respectively. The relationship between reflectance and soil properties, however, degrades when going from the laboratory scale to the field and large scales, due to the variations in surface status including roughness, soil moisture and nature of pebbles (Lagacherie et al., 2008).

Sullivan (2005) used Multiple linear regression analyses to relate RS data to soil properties in conventionally tilled fields of Alabama. regression estimates explained 0.11 to 0.61 of the variability in Total Carbon content using primarily red and NIR spectra of IKONOS multispectral data. Estimates of clay content using these RS data explained 0.34 to 0.55 of the variability.

High spatial resolution imagery is appropriate for investigating the sedimentation process in the flood spreading basins, because it provides more detailed information. Some satellites provide panchromatic images. High spatial resolution is the most important feature of PAN data (Hoppus et al., 2002). These images are essential in developing detailed and accurate maps and effectively planning fieldwork and they can create better discrimination between different land cover classes (Mei et al., 2005; Rao et al., 2002). Also they can be used to enhance the quality of images with lower spatial resolution (Licciardi et al., 2011). IRS high-resolution panchromatic satellite images have been available since 1997 when the IRS1D launched. The PAN images of these series of satellites can be high resolution resources for monitoring spatial and temporal changes on land surfaces.

This study attempts to assess the sedimentation process in the basins of Dahandar flood spreading system by using PAN data of IRS satellites and for achieving this purpose different classification methods and regression analysis were used in order to determine the dispersion, texture and thickness of sediments.

2. Materials and methods

2.1. Study area

Hasht bandi plain is located 60 km east of Minab city in south of Iran. The eastern part of this plain is bordered by Dahandar mountains. Dahandar ephemeral river originates from these mountains and runs in the northern part of Hasht bandi plain. The river basin has a total area of approximately 213.56 km^2 and the mean annual runoff of it is 12800000 m^3 (Moslemi et al., 2017). As the river flows downstream, it spreads out over the area and gets broken into separate parts and eventually most of it evaporates (Fig. 1). The climate of this region is hot and dry and the annual rainfall is about 197 mm. The highest mean temperature of the region is 35.3 ˚c in July and the lowest mean temperature is 19 ˚c in January. The mean altitude of the plain is 320 m and the slope average of the area is approximately 1.5%. The domain soil orders in the region according to soil taxonomy are Aridisols and Entisols. The soil moisture regime and temperature regime are aridic and hyperthermic respectively. Geoelectric studies have shown that Hasht bandi plain has an unconfined aquifer. The region is located between Sanandaj-Sirjan and Makran geological zones and contains an up to 52-m-thick sedimentary record of Quaternary sand and clay deposits (Moslemi et al., 2017). 95% of Hasht bandi residents are farmer and unfortunately in recent years, the volume of groundwater in storage has decreased because of excess groundwater pumping. Hormozgan province organization for natural resources management built Dahandar flood water spreading system between 2001 until2005 along Dahandar ephemeral river, in order to increase the natural supply of groundwater. Dahandar flood water spreading system is constructed in two phases (Fig. 1). The basins of the second phase are better arranged and organized, between 27˚ 10′ 0.2″ to 27˚ 11′ 1.17″N and 57˚ 30′ 55.8″ to 57˚ 32′ 5.71″ E, so this study is done based on it.

2.2. Field soil sampling

For determining soil texture, samples were collected from top soil layer (0–5 cm depth) every 50 m along the flood spreading system by

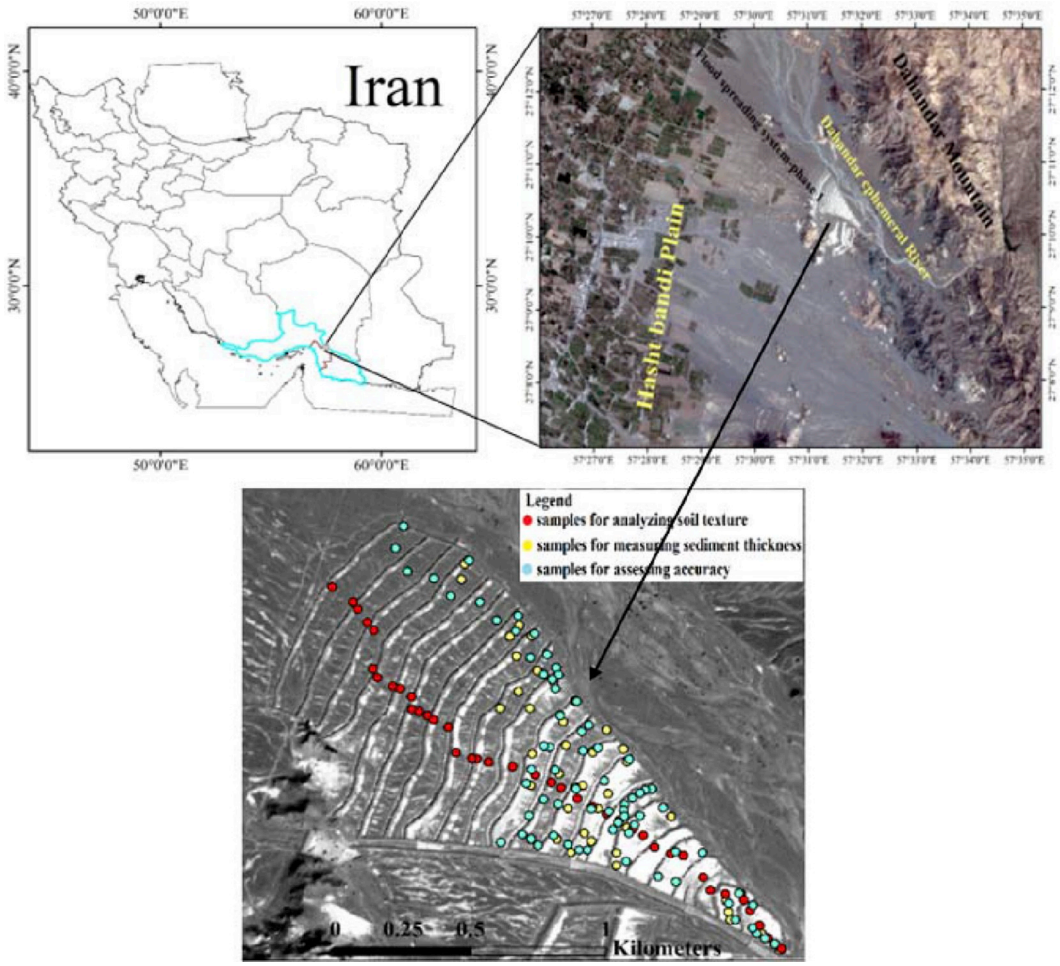

Fig. 1. Dahandar flood spreading system in south of Iran and soil ground sampling locations.

Fig. 2. The interconnected basins and conveyance channel of Dahandar flood spreading system.

using systematic random sampling technique (Fig. 1). Then the soil samples passed through a 2 mm sieve, prior to laboratory analysis. In laboratory, the percentages of sand, silt and clay for each sample were determined by using hydrometer method (Bouyoucos, 1936). then, the soil texture of every sample was determined based on the USDA soil texture triangle. For testing the thickness of deposited sediment layer, another various points were selected at different basins and corresponding thickness at each point was measured by a long ruler (Table 1).

2.3. Image data and image processing

2.3.1. Image data

Three series of IRS(P5) panchromatic band data were taken from National Geographical Organization of Iran. The scenes acquired on 5-Oct-2007, 01-Nov-2010, 13-Dec-2016 and all of them have a spatial resolution of 2.5 m and the spectral band is between 500 until 850 nm. The images georeferenced using WGS84 coordinate system (Fig. 3).

2.3.2. Developing classified maps

Based on the latest panchromatic image, Different supervised classification techniques (Minimum distance- Maximum likelihood- Piped) were used for determining the most suitable maps for soil texture and sediment thickness all over the flood spreading system (Tempfli et al., 2009). four maps for every soil property and a total of 20 maps were prepared by using IDRISI Selva software. Training sites were selected based on the percentages of sand, clay and silt in the soil samples. For instance, four categories (0–25%, 26%–50%, 51%–75% and 76%–100%) were considered as training sites for sand content. and for developing classified maps related to the thickness of deposited sediment layer, training sites were developed by dividing sediment thickness values into different categories (less than 1 cm, between 1 cm and 5 cm, between 5 cm and 10 cm and more than 10 cm).

2.4. Regression analysis

Regression analysis was used for finding the amount of relationship between sand, silt and clay contents of 40 soil samples and

Table 1
Measured soil properties using hydrometer method and USDS soil texture triangle.

Sample No	Clay (%)	Silt (%)	Sand (%)	DN	Soil texture
1	28	58	14	177	silty clay loam
2	4	30	66	152	sandy loam
3	22	40	38	142	loam
4	18	80	2	159	silt loam
5	32	30	38	143	clay loam
6	2	14	84	130	loamy sand
7	38	42	20	183	silty clay loam
8	8	32	60	177	sandy loam
9	14	72	14	171	silt loam
10	36	29	35	199	clay loam
11	24	62	14	198	silt loam
12	30	42	28	188	clay loam
13	6	16.6	77.4	165	loamy sand
14	0	16	84	129	loamy sand
15	4	74	22	185	silt loam
16	2	12	86	147	loamy sand
17	28	42	30	163	clay loam
18	20	44	36	138	loam
19	38	48	14	178	silty clay loam
20	4	64	32	179	silt loam
21	18	32	50	179	loam
22	20	72	8	188	silt loam
23	12	36	52	143	loam
24	26	38	36	188	loam
25	20	62	18	183	silt loam
26	6	20	74	168	sandy loam
27	38	32	30	195	clay loam
28	2	20	78	128	loamy sand
29	10	74	16	178	silt loam
30	2	6	92	140	sand
31	2	4	94	127	sand
32	18	26	56	184	sandy loam
33	28	38	34	168	clay loam
34	4	14	82	144	loamy sand
35	18	24	58	176	sandy loam
36	34	56	10	187	silty clay loam
37	4	14	82	129	loamy sand
38	0	10	90	132	sand
39	44	30	26	124	clay
40	26	58	16	185	silt loam

corresponding digital numbers (DNs) of latest IRS(P5) image (Liao et al., 2013). The method was used for checking the amount of correlation between sediment thickness and corresponding DNs too, based on the locations that were mentioned earlier. The output results were a series of linear equations. The validation coefficient R^2 is also a good measure for representing regression effectiveness. In regression analysis of sediment thickness and DNs, four categories (less than 1 cm, between 1 cm and 5 cm, between 5 cm and 10 cm and more than 10 cm) were chosen as independent variables, because based on the observations that were carried out on the study area, it was considered this kind of classification could produce more precise results.

2.5. Evaluating the accuracy of the classified maps

For assessing the accuracy of classified maps, another 39 points were selected from all over the flood spreading system (fig. 1) and both surface sediment thickness and percentages of clay, sand and silt contents were measured. For selecting the best techniques to predict the type of surface soil texture and measuring thickness of surface sediment all over the flood spreading system, Overall accuracy formula was used $X = \left(\frac{t}{n}\right)*100$, (where t is the number of correct classified points and n is the total number of sampling points) (Congalton, 1991). The maps with higher percentage values offer better performance, this means that they can predict the described soil properties more precisely.

3. Results and discussion

3.1. Soil analysis

The results of hydrometer method are presented in Table 1. The maximum-minimum values for sand, silt and clay particles were (94%–2%), (80%–4%) and (44%–0%) respectively in the soil samples and the range of corresponding DNs of sample locations varied from 124 to 199 based on the latest IRS(P5) panchromatic image. As shown in soil texture triangle, some textures such as clay, silt, sandy clay, sandy clay loam almost did not exist on the flood spreading system surface (Fig. 4).

Sediment load components travel at different rates through the Alluvial system and are deposited in characteristic settings (Malmon et al., 2004). A large amount of sand particles gets deposited immediately, but silt has moderate deposition and clay has the lowest deposition rate (Lilhare et al., 2014). So the soil textures that contain both sand and clay particles were observed less than the other textures on the surface of flood spreading system.

3.2. Statistical analysis of remote sensing data

The type of sediment texture and spatially variable concentrations of it can create differences in reflectance, so remote sensing techniques can reveal particular sedimentation patterns in different environments. These monitoring techniques are used in order to define the relation between upstream soil erosion and downstream (coastal) water quality (Alexandridis et al., 2015), monitoring the suspended sediment concentrations in coastal lagoons (Kumar et al., 2016), characterizing surface sediment in desert areas (Gaber et al., 2015) and many other case studies. In this study 20 supervised classified maps were prepared for determining the spatial distribution of sediment thickness and percentages of sand, silt and clay particles by using four supervised classification algorithms include maximum likelihood, minimum distance-raw, minimum distance-normalized, parallelepiped (Figs. 5,6,7,8,9). By using overall accuracy, evaluation of the supervised classified maps was done and the performance of every algorithm was analyzed to assess how correctly the maps can discriminate the soil attributes in unknown

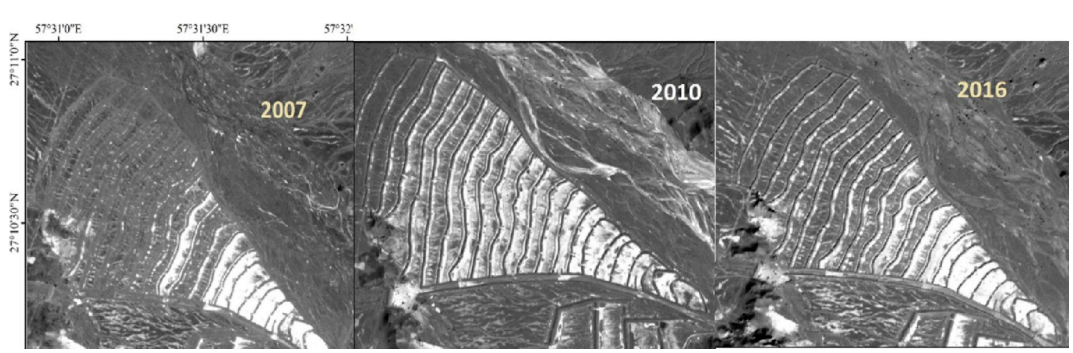

Fig. 3. Time series of IRS(P5) panchromatic image of the study area.

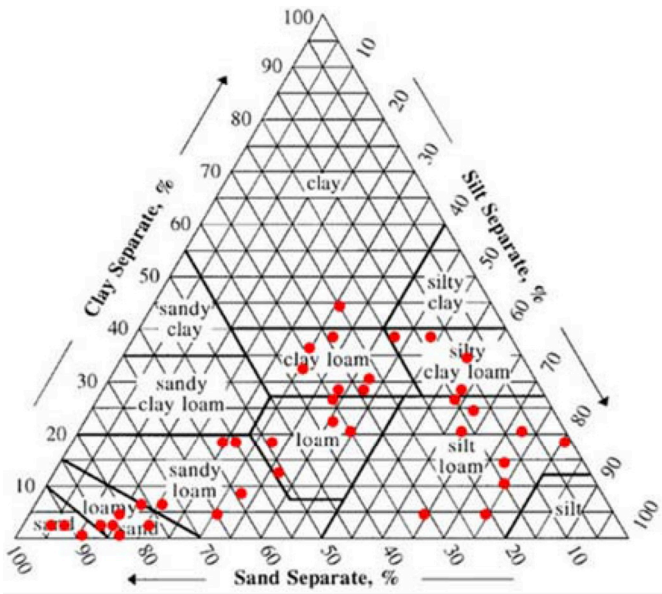

Fig. 4. Soil texture classification based on USDA classification system.

locations of Dahandar flood spreading system (Table 2).

3.2.1. Soil particles classification using algorithms

For sand particles, the map made by Maximum likelihood algorithm had the most appropriate overall accuracy with 64%, among the other classification algorithms (Table 2) and (Fig. 5). The accuracy of maximum likelihood algorithm is usually high for larger scale studies (Ali et al., 2018; Allam et al., 2019), but for smaller scale areas like evaluating flood spreading system sedimentation process, the accuracy of classified maps may decrease especially when the subject of classified maps is the distribution of percentage of sand, silt and clay particles. and it should be considered that although the accumulation of each particle is higher than the others in a specific area; sand, silt or clay particles are not completely separated from each other on the flood spreading systems. These can be some reasons for explaining the decrease in accuracy results. Minimum distance was the best method for preparing clay and silt distribution maps and the overall accuracies were 46% and 51% respectively (Table 2) and (Figs. 6 and 7). The result is different from Gaber et al. (2015) that used minimum distance algorithm for studying surface sediment in desert environment, although It should be considered that in the mentioned study, the scale of studying area and remote sensing data were different and the classified maps were made based on the distribution of gravel and sand.

3.2.2. Soil texture classification using algorithms

For assessing soil texture classification, parallelepiped algorithm showed the most accurate results (Table 2). There are 12 soil texture in USDA soil texture triangle, so by a little change in the percentage of sand, silt or clay contents, there would be a new soil texture. It seems that the variety of soil texture types has decreased the overall accuracy of algorithms. parallelepiped algorithm is a quick-look classifier and it creates boxes within the training sites. If a given pixel falls within a signature box, it is assigned to that category. Pixels that do not fall inside any of the boxes will be referred to as the reject class. Black areas are reject classes in the soil texture map that was created by parallelepiped algorithm (Richards, 1999; Tempfli et al., 2009) (Fig. 8). It seems that due to the large number of soil texture classes, parallelepiped algorithm has shown better results in compare to the other algorithms.

3.2.3. Sediment thickness classification using algorithms

The results of algorithms were close together for sediment thickness

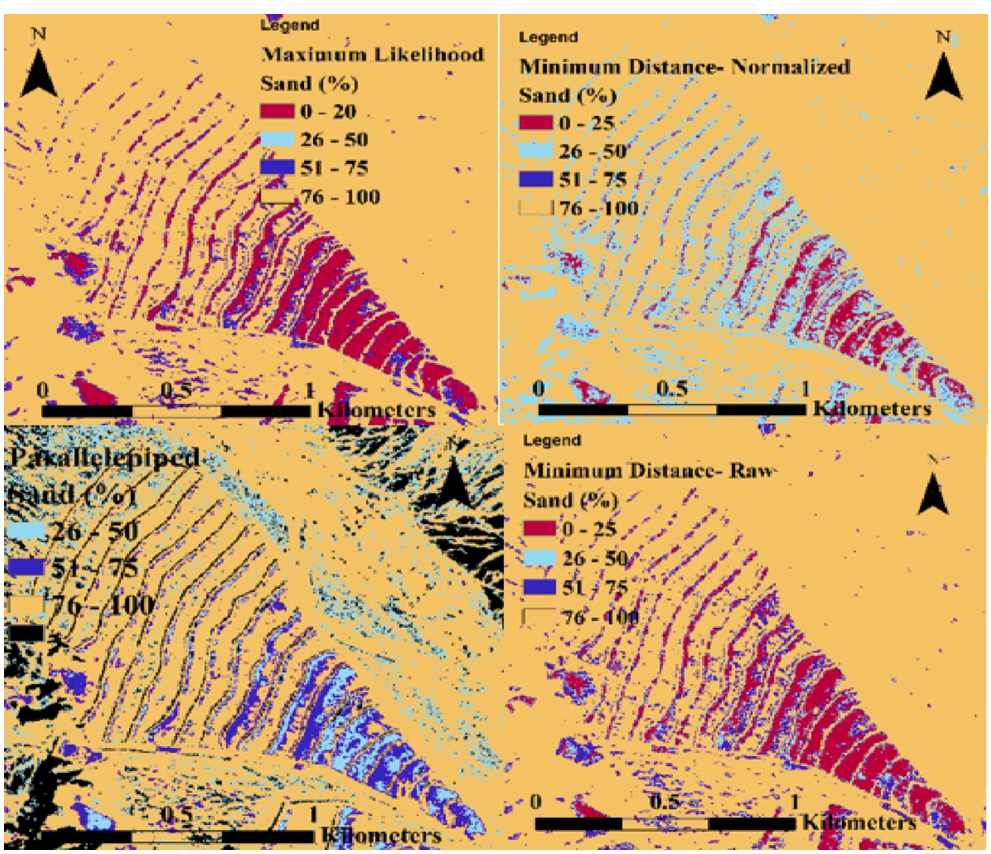

Fig. 5. Supervised Classification maps representing spatial distribution of sand particles.

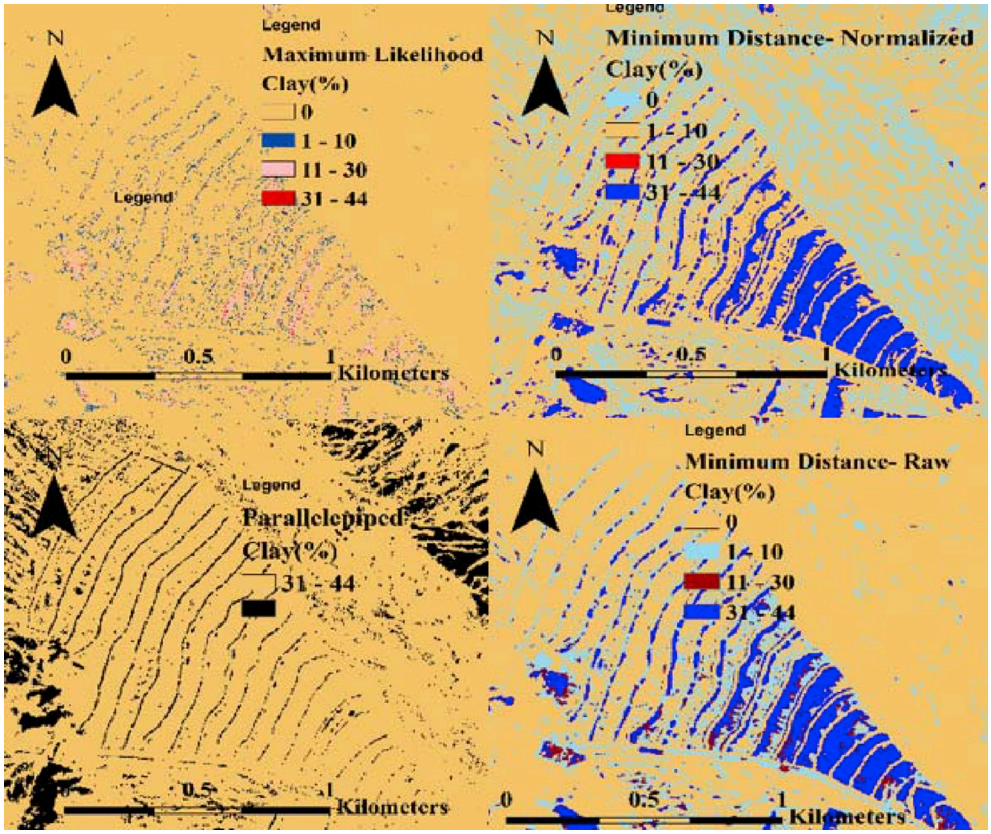

Fig. 6. Supervised classification maps representing spatial distribution of clay particles.

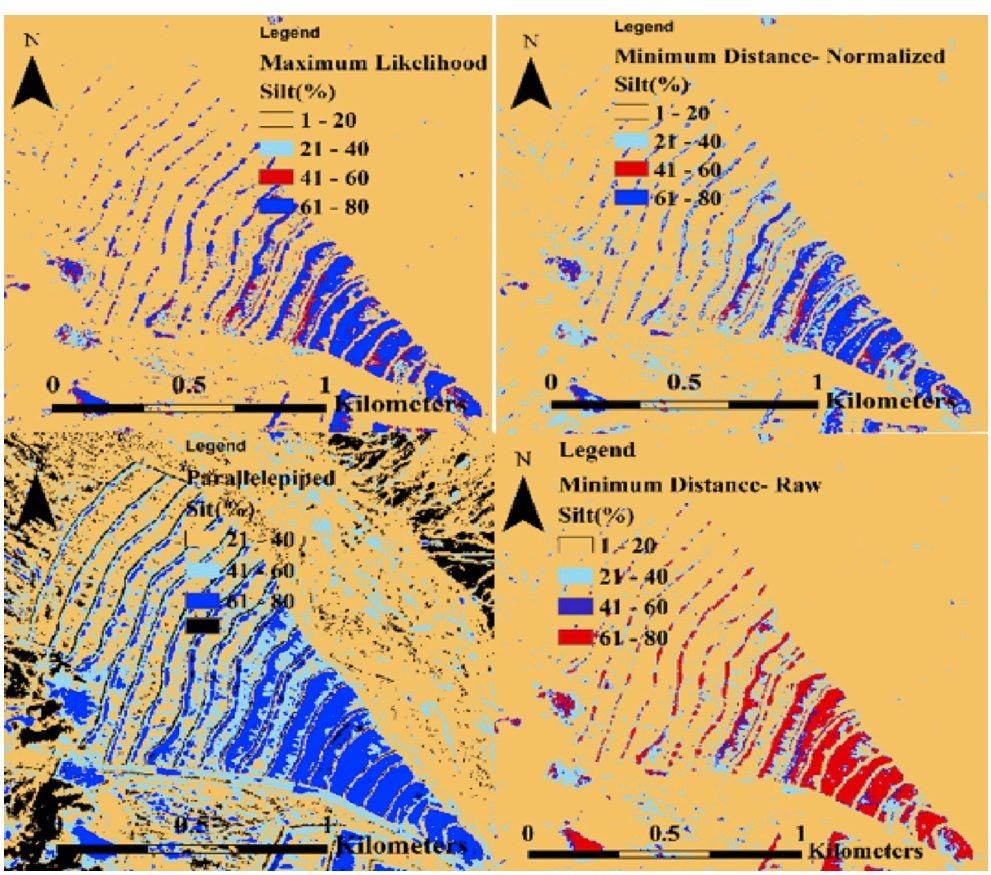

Fig. 7. Supervised classification maps representing spatial distribution of silt particles.

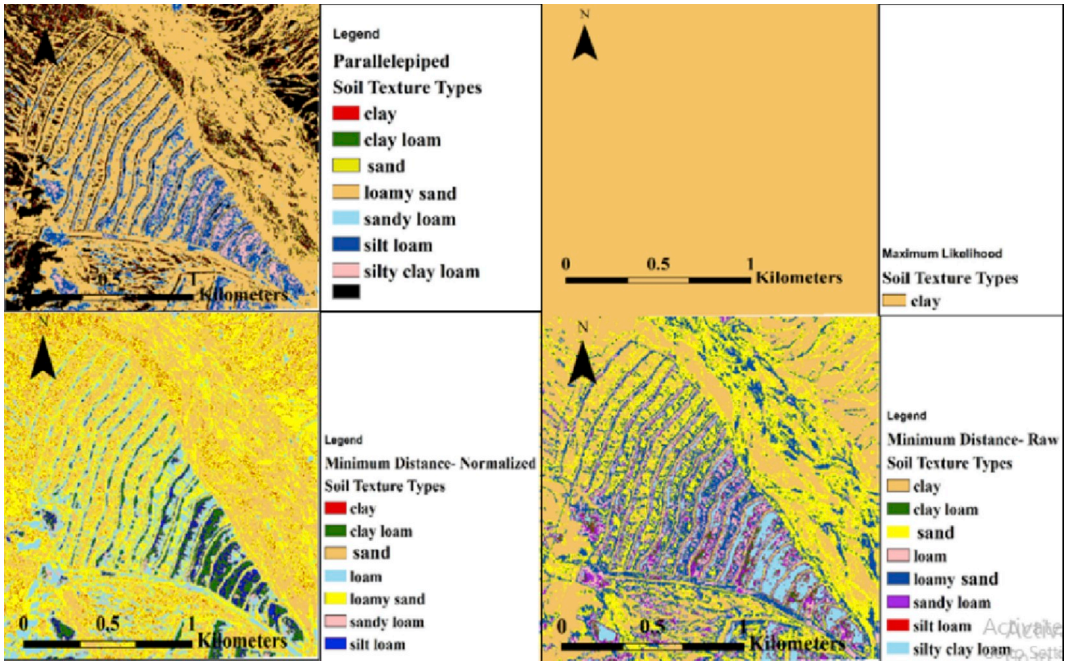

Fig. 8. Supervised Classification maps representing spatial distribution of different types of soil textures.

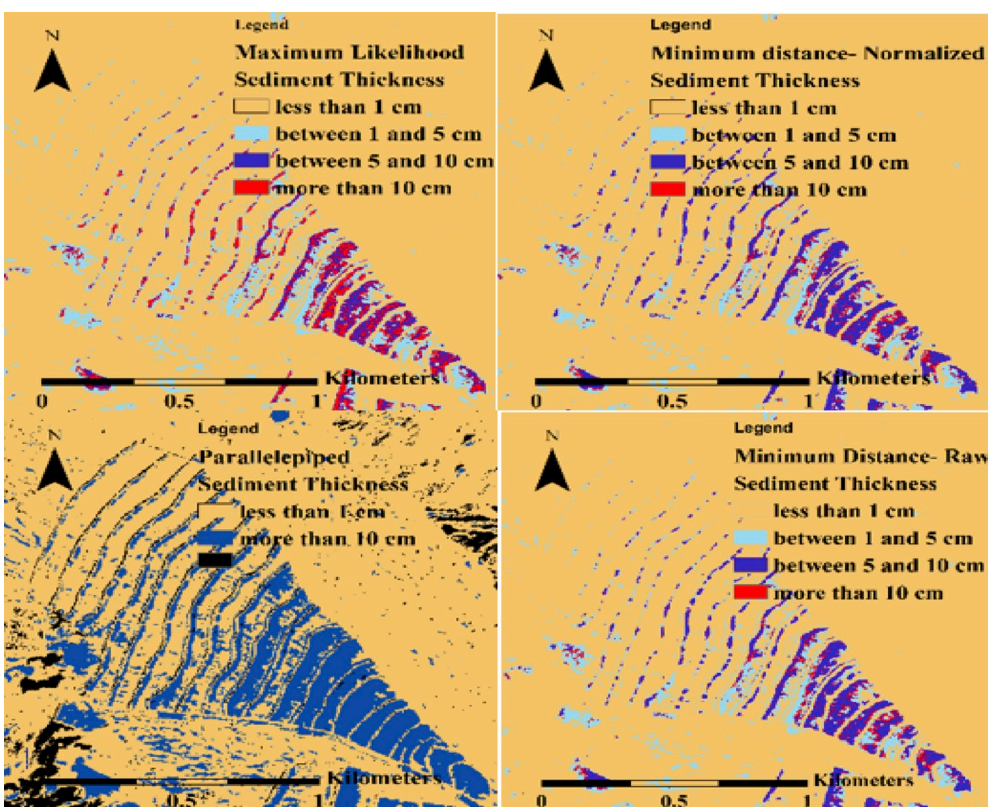

Fig. 9. Supervised Classification maps representing spatial distribution of sediment thickness.

classification (Table 2). For sediment thickness maps, the classes were: <1 cm, 1–5 cm, 5–10 cm, more than 10 cm (Fig. 9). The order of this categorization is different from the other soil properties. Probably selecting this kind of categorization has increased the accuracy results.

3.3. Mapping and characterizing surface sediment

Fig. 5 shows that the highest percentage of sand content (76%–100%) is located in areas without sediment and the soil of area that the flood spreading system is built on it. Figs. 6 and 7 indicate clay and silt particles are totally distributed in first basins that most of sedimentation process has occurred in them. According to soil texture map that is made

Table 2
Overall accuracy values representing the performance of algorithms used for generating the supervised classification maps.

	Minimum distance (raw)	parallelepiped	Minimum distance (normalized)	Maximum likelihood
soil texture	23%	28%	7%	–
sand	56%	38%	53%	64%
clay	43%	12%	46%	30%
silt	51%	33%	48%	41%
Sediment thickness	53%	53%	56%	56%

by parallelepiped algorithm, the soil textures that are seen in the surface sediments of first basins are silty clay loam and silt loam, but sand and loamy sand are the soil textures that are seen in the next basins that have less sediment load. Different maps in Fig. 8 show sediment thickness between 5 and 10 cm is mostly observed in the first basins and in the most parts of subsequent basins that sediment load has transferred less to those areas, sediment thickness is less than 1 cm (Fig. 9). Field investigations confirmed these findings too (Fig. 10). When floodwater spreads on the ground most of suspended sediment settles on the bottom of the first basins. For subsequent basins of the flood spreading system, the thick sediment layer is mostly observed on the edge of basins (Fig. 10). IRS image of Fig. 10 shows clearly the pattern of sedimentation. As it can be seen in this picture, the color of sedimentation parts that are mostly in the first ten basins and on the edge of subsequent basins, seems lighter than areas without sediment. As mentioned before, most of surface sediment consists of clay and silt particles. these particles are finer than sand so recharge rates will decrease as a result of the accumulation of them on the flood spreading system soil which is composed of the highest percentages of sand content. by occurring continuous flood events the thickness of sediment increase, and this is so significant in reducing recharge rates, especially when the sedimentation thickness reaches to higher than 5 cm that is a noticeable thickness for reducing recharge rates. So desiltation operation for improving the efficiency of the first basins infiltration seems totally necessary.

3.4. Regression analysis

Soil spectral response curves are used in soil studies and it provides more strong relationship with soil properties (Lagacherie et al., 2008), but corresponding DNs can provide more straight results. Simple linear regression was used for determining the relationship between the percentages of sand, silt, clay contents and surface sediment thickness with corresponding DNs of 2016 panchromatic image. The results are shown in Fig. 2. The relationships between clay and silt contents and Surface sediment thickness with DNs were positive although this relationship for sand particles was negative (Fig. 11). The R^2 values of regression analysis were 0.4282, 0.2274, 0.3439 and 0.4295 for sand, clay, silt and sediment thickness respectively (Table 3). Sand particles provide higher R^2 value in compare to silt and clay R^2 values besides silt R^2 value was higher than clay particles. These findings are slightly different from the results that obtained by (Li et al., 2014; Liao et al., 2013). In Liao et al. (2013) study, the relationship between sand, silt and clay content with DNs of band 7 of Landsat ETM + imagery were evaluated and the R^2 values were 0.32, 0.21 and 0.36. Also the relationship between sand content and DNs was positive, but negative for the other variables. Li et al. (2014) studied the relationship between percentages of sand, silt and clay particles with reflectance of Landsat (TM4) and the R^2 values were 0.66, 0.62 and 0.64. The relationship was only negative for sand content.

Sediment thickness values categorized into 4 groups (<1 cm, 1–5 cm, 5–10 cm, >10 cm) and simple linear regression was applied between the groups and DNs (Fig. 11). The results indicated 0.429 for R^2 value in sediment thickness regression analysis, that is higher than the other soil properties R^2 values.

4. Conclusion

IRS panchromatic images with 2.5m resolution were used for assessing the sedimentation process on Dahandar flood spreading system. Simple linear regression analysis revealed that sand particles and sediment thickness had better correlation with DNs compared to the other soil properties and the relationship between sand particles and DNs was negative. R^2 values of the regression analysis were 0.42, 0.22, 0.34 and 0.42 for sand, clay, silt and sediment thickness. For sand particles maximum likelihood, for clay and silt minimum distance and for soil texture map parallelepiped algorithms with respectively 64%, 46%, 51% and 28% overall accuracy had the best performance. The results of algorithms were close together for sediment thickness classification. Higher percentages of silt and clay contents and 5–10 cm sediment thickness class, with silty clay loam and silt loam soil textures were seen

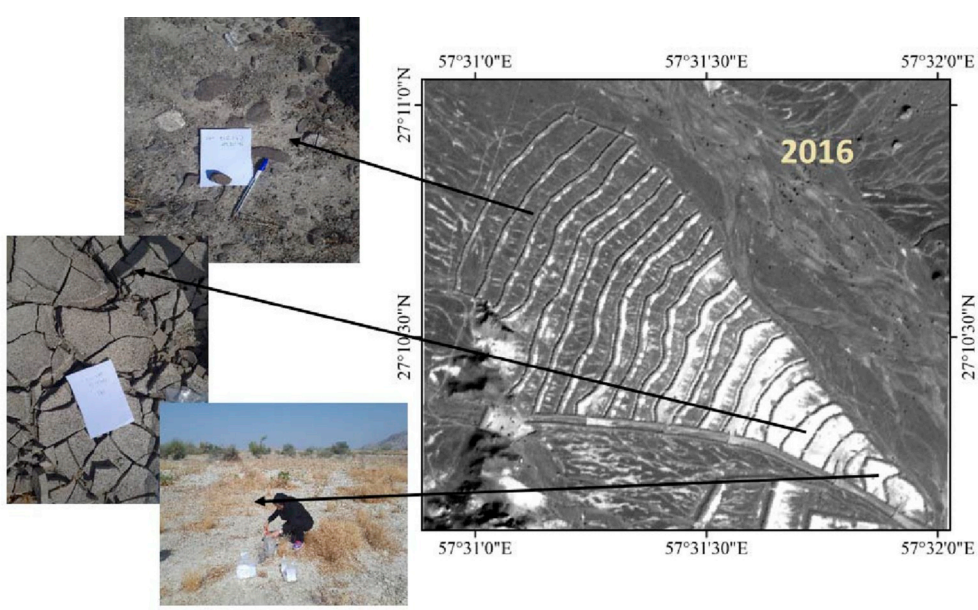

Fig. 10. Changes in sediment thickness and soil particle distribution at different basins of the flood spreading system.

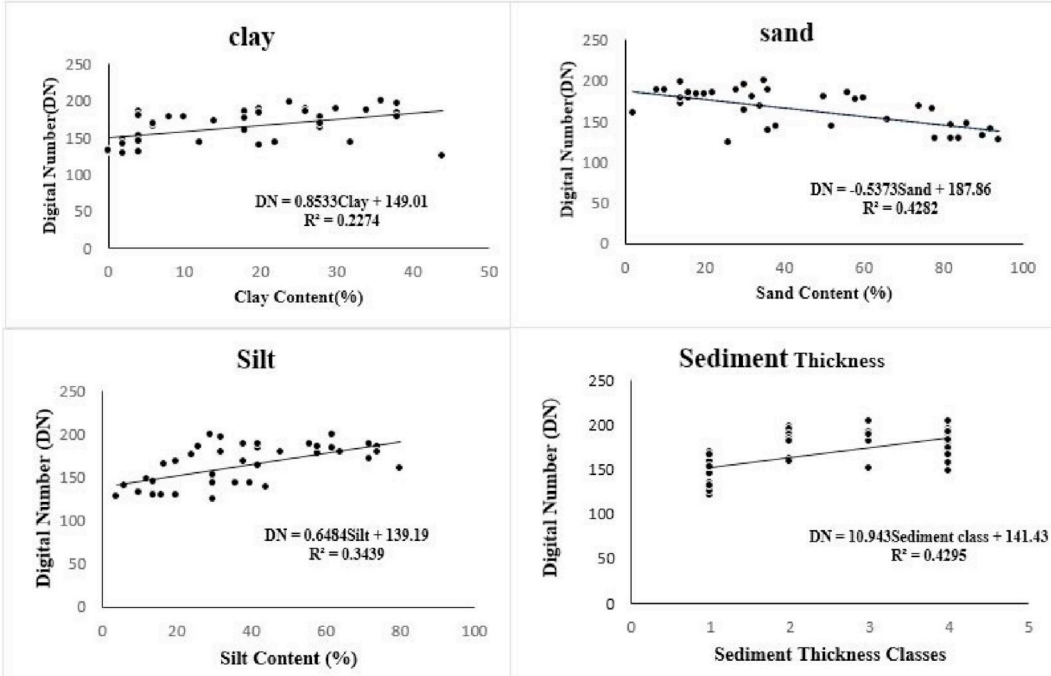

Fig. 11. Scatter plots obtained by regression analysis between soil properties and corresponding DNs.

Table 3
R^2 values and regression equations between sediment thickness, surface soil sand, silt and clay contents with DNs of IRS(P5) panchromatic imagery.

Soil properties	regression equation	R2
Sand	Y = −0.5373DN+187.86	0.4282
Clay	Y = 0.8533DN+149.01	0.2274
Silt	Y = 0.6484DN+139.19	0.3439
Sediment Thickness	Y = 10.943DN+141.43	0.4295

in most of sediment deposition areas and the areas without sediment deposition mostly contained sand particles and <1 cm sediment thickness class with sand and loamy sand soil textures. Although the overall accuracy and R^2 values were low, in general IRS panchromatic images by using simple linear regression analysis and common supervised classification algorithms had reasonably assessed the sedimentation process all over Dahandar flood spreading system.

Appendix A. Supplementary data

Supplementary data to this article can be found online at https://doi.org/10.1016/j.rsase.2019.100269.

References

Alexandridis, T.K., Monachou, S., Skoulikaris, C., Kalopesa, E., Zalidis, G.C., 2015. Investigation of the temporal relation of remotely sensed coastal water quality with GIS modeled upstream soil erosion. Hydrol. Process. 29, 2373–2384.

Ali, M.Z., Qazi, W., Aslam, N., 2018. A comparative study of ALOS-2 PALSAR and landsat-8 imagery for land cover classification using maximum likelihood classifier. Egypt.J. Remote.Sens.Space Sci. 21, S29–S35. https://doi.org/10.1016/j.ejrs.2018.03.003.

Allam, M., Bakr, N., Elbably, W., 2019. Multi-temporal assessment of land use/land cover change in arid region based on landsat satellite imagery: case study in fayoum region, Egypt. Remote Sens.Appl.: Soc.Environ. 14, 8–19.

Bahadur Kc, K., 2009. Improving landsat and IRS image classification: evaluation of unsupervised and supervised classification through band ratios and DEM in a mountainous landscape in Nepal. Remote Sens. 1, 1257–1272. https://doi.org/10.3390/rs1041257.

Bartholdy, J., Folving, S., 1986. Sediment classification and surface type mapping in the Danish Wadden Sea by remote sensing. Neth. J. Sea Res. 20 (4), 337–345. https://doi.org/10.1016/0077-7579(86)90001-3.

Bouyoucos, G.J., 1936. Directions for making mechanical analysis of soils by the hydrometer method. Soil Sci. 42, 225–230. https://doi.org/10.1097/00010694-193609000-00007.

Congalton, R.G., 1991. A review of assessing the accuracy of classifications of remotely sensed data. Remote Sens. Environ. 37 (1), 35–46. https://doi.org/10.1016/0034-4257(91)90048-B.

Demattè, J.A.M., Alves, M.R., Terra, F.d.S., Bosquilia, R.W.D., Fongaro, C.T., Barros, P.P. d.S., 2016. Is it possible to classify topsoil texture using a sensor located 800 km away from the surface? Rev. Bras. Ciência do Solo 40, 1–13.

Duda, T., Canty, M., 2002. Unsupervised classification of satellite imagery: choosing a good algorithm. Int. J. Remote Sens. 23 (11), 2193–2212. https://doi.org/10.1080/01431160110078467.

Fennemore, G.G., Davis, A., Goss, L., Warrick, A.W., 2005. A rapid screening-level method to optimize location of infiltration ponds. Gr. Water 39 (2), 230–238. https://doi.org/10.1111/j.1745-6584.2001.tb02304.x.

Gaber, A., Koch, M., El-Baz, F., 2009. Textural and compositional characterization of wadi feiran deposits, sinai peninsula, Egypt, using radarsat-1, PALSAR, SRTM and ETM+ data. Remote Sens. 2 (1), 52–75.

Gaber, A., Soliman, F., Koch, M., El-Baz, F., 2015. Using full-polarimetric SAR data to characterize the surface sediments in desert areas: a case study in El-Gallaba Plain, Egypt. Remote Sens. Environ. 162, 11–28. https://doi.org/10.1016/j.rse.2015.01.024.

Hashemi, H., Berndtsson, R., Persson, M., 2013. Floodwater harvesting for artificial recharge and spate irrigation in arid area. Vatten: tidskrift för vattenvård /Journal of Water Management and research 69 (2), 93–100.

He, T., Wang, J., Lin, Z., Cheng, Y., 2009. Spectral features of soil organic matter. Geo Spat. Inf. Sci. 12 (1), 33–40. https://doi.org/10.1007/s11806-009-0160-x.

Hoppus, M.L.R., Rachel, I., Lister, Andrew J., Finco, Mark V., 2002. April 8-12, 2002). *The effectiveness of texture analysis for mapping forest land using the panchromatic bands of Landsat 7, SPOT, and IRS imagery*. In: Paper Presented at the Proceedings of the Ninth Forest Service Remote Sensing Applications Conference (San Diego, CA).

Jimenez, L.O., Rivera-Medina, J., Rodríguez-Díaz, E., Arzuaga, E., Ramirez, M., 2005. Integration of spatial and spectral information by means of unsupervised extraction and classification for homogenous objects applied to multispectral and hyperspectral data. Geosci. Remote Sens.IEEE Trans. 43, 844–851. https://doi.org/10.1109/TGRS.2004.843193.

Kowsar, A., 1991. Floodwater spreading for desertification control: an integrated approach. Desertif. Control Bull. 19, 3–18.

Kumar, A., Equeenuddin, S.M., Mishra, D.R., Acharya, B.C., 2016. Remote monitoring of sediment dynamics in a coastal lagoon: long-term spatio-temporal variability of suspended sediment in Chilika. Estuar. Coast Shelf Sci 170, 155–172. https://doi.org/10.1016/j.ecss.2016.01.018.

Lagacherie, P., Baret, F., Feret, J.-B., Madeira Netto, J., Robbez-Masson, J.M., 2008. Estimation of soil clay and calcium carbonate using laboratory, field and airborne hyperspectral measurements. Remote Sens. Environ. 112 (3), 825–835. https://doi.org/10.1016/j.rse.2007.06.014.

Li, H., Zhang, C., Gong, Z., 2014. Mapping sediment types of muddy intertidal zone by means of TM remote sensing image. Indian J.Geo-Marin.Sci. 43 (10), 1849–1856.

Liao, K., Xu, S., Wu, J., Zhu, Q., 2013. Spatial estimation of surface soil texture using remote sensing data. Soil Sci. Plant Nutr. 59 (4), 488–500.

Licciardi, G.A., Khan, M.M., Chanussot, J., Montanvert, A., Condat, L., Jutten, C., 24-29 July 2011. Fusion of Hyperspectral and panchromatic images using multiresolution analysis and nonlinear PCA band reduction. In: Paper Presented at the 2011 IEEE International Geoscience and Remote Sensing Symposium.

Lilhare, R., Garg, V., Nikam, B., 2014. Application of GIS-coupled modified MMF model to estimate sediment yield on a watershed scale. J. Hydrol. Eng. 20. P.C5014002. DOI: 10.1061/(ASCE)HE.1943-5584.0001063.

Lu, D., Mausel, P., Brondízio, E., Moran, E., 2004. Change detection techniques. Int. J. Remote Sens. 25 (12), 2365–2401. https://doi.org/10.1080/0143116031000139863.

Lu, D., Weng, Q., 2007. A survey of image classification methods and techniques for improving classification performance. Int. J. Remote Sens. 28 (5), 823–870. https://doi.org/10.1080/01431160600746456.

Madden, R.H.C., Wilson, M.E.J., O'Shea, M., 2013. Modern fringing reef carbonates from equatorial SE Asia: An integrated environmental, sediment and satellite characterisation study. Mar. Geol. 344, 163–185 (Supplement C).

Malmon, D.V., Steve, L.R., Thomas, D., 2004. Sediment sorting and transport by flash floods. J. Geophys. Res.: Earth Surface 109 (F2). https://doi.org/10.1029/2003JF000067.

Mei, S., Fenton, M., Paulen, R., 2005. *Integration Of Remote-Sensing and Geological Data as Aids to Mapping Surficial Sediments in Northwestern Alberta*. Technical Report, Report Number: AGS Earth Science Report 2005-03, Affiliation. Alberta Geological Survey. M.

Moazami, M., Zoratipour, A., 2016. Determining sedimentation trend on flood spreading system using satellite image change detection technique. J.Water Soil Conserv. 23 (2), 211–214. https://doi.org/10.22069/JWFST.2016.3064.

Moghanlou, K.M., Oskouei, A.K., 2007. Investigation of quaternary deposits suitable for floodwater spreading. In: Paper Presented at the International Congress of River Basin Management (Antalya, Turkey).

Moslemi, H., Abkar, A., Choopani, S., 2017. Assessment the effects of dehender flood spreading on groundwater resources in Hashtbandi plain, Hormozgan province. J. Watershed. Eng. Manag. 8 (Issue 4), 377–388.

Mostafaei, A., Kalantari, N., Zarkesh, M.K., 2016. Assessing the success of floodwater spreading projects using a fuzzy approach. Water Sci. Technol. 74 (8), 1980–1991. https://doi.org/10.2166/wst.2016.394.

Muller, S.J., van Niekerk, A., 2016. An evaluation of supervised classifiers for indirectly detecting salt-affected areas at irrigation scheme level. Int. J. Appl. Earth Obs. Geoinf. 49, 138–150. https://doi.org/10.1016/j.jag.2016.02.005.

Munyati, C., 2019. Comparative performance of regression tree and parametric classification of savannah woody cover on SPOT 6 NAOMI imagery. Remote Sens. Appl.: Soc.Environ. 13, 171–182. https://doi.org/10.1016/j.rsase.2018.10.015.

Nanni, M., Demattê, J.A., 2006. Spectral reflectance methodology in comparison to traditional soil analysis. Soil Sci. Soc. Am. J. 70 (2), 393–407. https://doi.org/10.2136/sssaj2003.0285.

Rao, P.V.N., Sai, M.V.R.S., Sreenivas, K., Rao, M.V.K., Rao, B.R.M., Dwivedi, R.S., Venkataratnam, L., 2002. Textural analysis of IRS-1D panchromatic data for land cover classification. Int. J. Remote Sens. 23 (17), 3327–3345. https://doi.org/10.1080/01431160110104665.

Richards, J.A., 1999. Remote Sensing Digital Image Analysis: an Introduction. Springer-Verlag Berlin, Heidelberg.

Shaharum, N.S.N., Shafri, H.Z.M., Gambo, J., Abidin, F.A.Z., 2018. Mapping of Krau Wildlife Reserve (KWR) protected area using Landsat 8 and supervised classification algorithms. Remote Sens.Appl.: Soc.Environ. 10, 24–35. https://doi.org/10.1016/j.rsase.2018.01.002.

Small, C., Steckler, M., Seeber, L., Akhter, S., Goodbred, S., Mia, M., Imam, B., 2009. Spectroscopy of sediments in the Ganges-Brahmaputra delta: spectral effects of moisture, grain size and lithology. Remote Sens. Environ. 113 (2), 342–361.

Sullivan, D.G., 2005. IKONOS imagery to estimate surface soil property variability in two Alabama physiographies. Soil Sci. Soc. Am. J. 69 (6), 1789–1798.

Tempfli, K., Huurneman, G.C., Bakker, W., Janssen, L.L.F., Feringa, W.F., Gieske, A., Woldai, T., 2009. Principles of Remote Sensing : an Introductory Textbook. Enschede, Netherland, pp. 280–305. ITC Educational Textbook Series.

Vasava, H.B., Gupta, A., Arora, R., Das, B.S., 2019. Assessment of soil texture from spectral reflectance data of bulk soil samples and their dry-sieved aggregate size fractions. Geoderma 337, 914–926. https://doi.org/10.1016/j.geoderma.2018.11.004.

Zarkesh, M.K., 2005. Decision Support System for Floodwater Spreading Site Selection in Iran. Thesis, (degree of doctor). Wageningen University, ITC, Enschede, Netherland.